Structure and Volumetric Properties of Linear and Triarm Star Polyethylenes from Atomistic Monte Carlo Simulation Using New Internal Rearrangement Moves

Loukas D. Peristeras,[†] Ioannis G. Economou,[†] and Doros N. Theodorou*[,†,‡]

Molecular Modeling of Materials Laboratory, Institute of Physical Chemistry, National Research Center for Physical Sciences "Demokritos", GR-153 10 Aghia Paraskevi, Attikis, Greece, and Department of Materials Science and Engineering, School of Chemical Engineering, National Technical University of Athens, 9 Heroon Polytechniou Street, GR-157 80 Athens, Greece

Received August 9, 2004; Revised Manuscript Received September 17, 2004

ABSTRACT: A number of elementary Monte Carlo moves are introduced for branched chain molecules. More specifically, branch point flip brings about a displacement in space of a branch point and its neighboring atoms in the molecule without change in the connectivity. Furthermore, branch point slithering allows for branch point displacement along the backbone; in this case, the size of the branches involved is changed. Finally, the flip move is extended to a dimer and is further generalized to an *n*-mer segment. The new Monte Carlo moves are used together with previously developed moves for the study of structure and volumetric properties of melts composed of symmetric triarm star polyethylenes of different arm lengths in a united atom representation. It is shown that the new moves result in very efficient relaxation of the macromolecules and, in particular, of their branch points. Comparisons are made against simulation results and experimental data for linear and branched polyethylene. The agreement between experimental data and Monte Carlo simulation for the melt density is good in all cases.

1. Introduction

In-depth understanding of molecular mechanisms and phenomena that affect macroscopic properties of polymers is crucial for the optimal design of novel materials for a variety of applications. A number of experimental methods, such as small-angle neutron scattering (SANS), small-angle X-ray scattering (SAXS), small-angle light scattering (SALS), and solid-state NMR, have advanced to a level that enables detailed elucidation of polymer microscopic structure.[1−6] Most of these methods are still quite expensive to use and require special pretreatment of the material. For the case of polyolefin blends, for example, deuteration of one of the components is needed in order to identify the signal of each component.

On the other hand, molecular simulation is a reliable tool for the determination of molecular structure and calculation of macroscopic thermodynamic, transport, mechanical, electrical, and other properties. In this way, accurate structure−property relationships can be established. Polymer systems have very long characteristic times for molecular relaxation that cannot be captured using brute force molecular dynamics. An alternative widely used method for such purposes is Monte Carlo simulation. In this case, appropriate "elementary" moves are needed so that important configurations are sampled efficiently.

In recent years, a number of elementary moves were designed specifically for long chain molecules. In the reptation move, an end segment of a randomly selected chain is cut off and appended to the other end with a randomly selected torsion angle.[7] In the configurational bias (CB) method, a terminal part (on the order of three to six segments) of a randomly selected chain is excised and removed. Subsequently, the removed part is regrown segment by segment in a biased way, by accounting for the energetic interactions with neighboring segments in the same or different chains. The bias introduced in this case is removed from the system using appropriate acceptance criteria.[8−10] Finally, in the flip move an inner atom of the chain is displaced along the locus defined by the lengths of the two bonds adjacent to the atom.[11] This move introduces local fluctuations in the configuration of chain molecules. It requires little computing time and has a large acceptance ratio.

As the chain size increases, efficient relaxation of the internal part of macromolecules becomes an important issue. A solution to the problem was proposed by Theodorou and co-workers based on the concerted rotation (CONROT) move.[12,13] In the general formulation of CONROT, a randomly selected internal trimer of skeletal atoms of the chain is excised. The two atoms neighboring the excised trimer are displaced through randomly selected changes to both torsion angles neighboring the trimer on its two sides. Finally, the trimer is reconstructed. In total, five skeletal segments are relocated and eight torsion angles are modified.

CONROT was further extended to moves involving multiple chains: in the end-bridging (EB) move[12,13] and recently in the double-bridging (DB) move.[14] These are very effective in sampling the long-range characteristics of long chains. The EB move induces polydispersity in the system a priori, and so a semigrand canonical ensemble formulation is required to control the chain length distribution. On the other hand, the DB move can be designed to preserve monodispersity. Using these very efficient moves, relaxation of important structural quantities, such as end-to-end distance and radius of gyration, for polymers of large molecular weight is possible.[15] Recently, intramolecular double bridging was

[†] National Research Center for Physical Sciences "Demokritos".
[‡] National Technical University of Athens
* To whom all correspondence should be addressed: e-mail doros@central.ntua.gr.

10.1021/ma048364p CCC: $30.25
Published on Web 12/21/2004

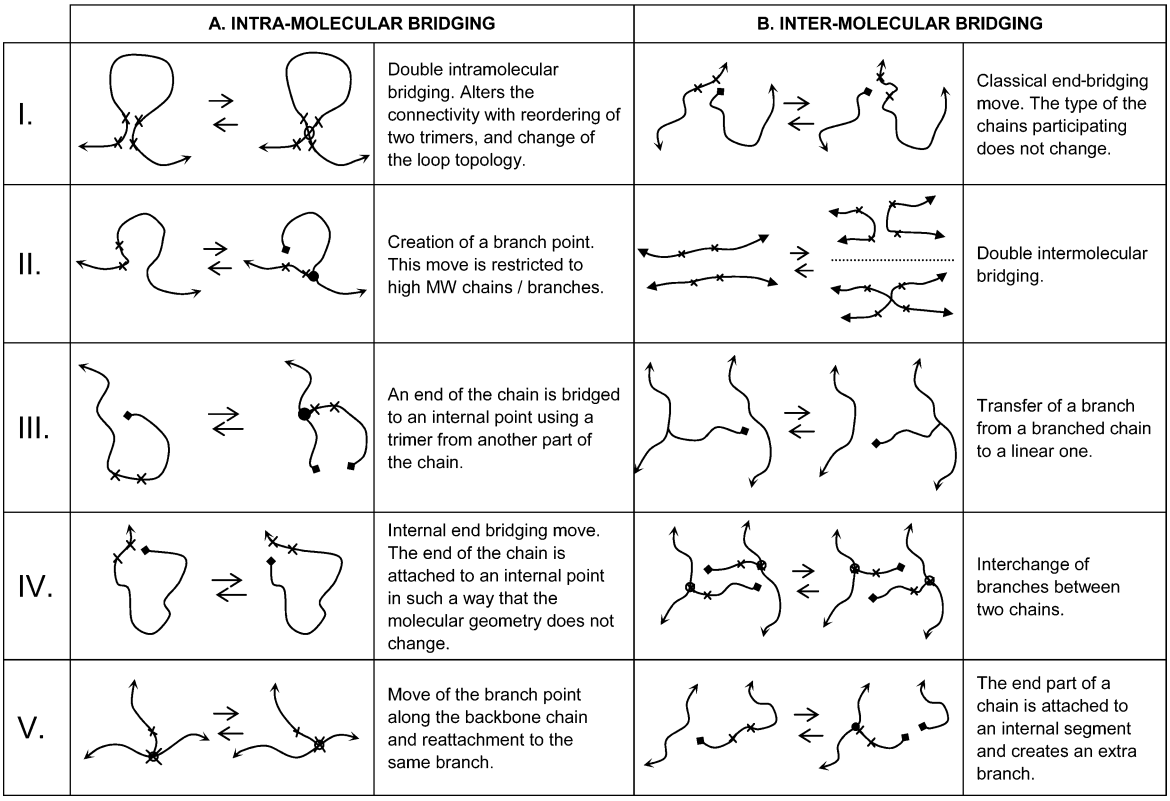

Figure 1. Schematic representation of various intramolecular and intermolecular bridging moves.

applied to H-shaped polymers (in short, H-BR move).[16]

In all the moves proposed so far (with the exception of H-BR), emphasis is given on the relaxation of the linear part of the chain molecule. This work focuses on long-branched polymers and, more specifically, on the efficient relocation of the branch point(s). Monte Carlo moves for the simulation of short-branched alkanes (e.g., methylalkanes) were proposed previously.[17,18] A number of new elementary moves are proposed for this purpose. The moves are developed for the semigrand canonical statistical ensemble and applied to a number of triarm star polyolefin melt systems at various temperatures. Efficient relaxation of the branch points and of the entire molecules is achieved. Microscopic structure and thermodynamic properties are reported for these branched polymers and compared to molecular simulation results for linear polyolefins. Finally, PVT properties for the triarm star polyolefin melts are reported.

2. Elementary Bridging Moves

The concept of local conformational rearrangement of complex molecules was introduced by Gō and Scheraga more than 30 years ago.[19] In the 1990s and 2000s, Theodorou and co-workers[12−15,20] extended this concept to continuum Monte Carlo simulation proposing the elementary moves known as CONROT, EB, and DB. In all cases, the underlying geometric problem is the determination of all possible ways to arrange in space a group of atoms, while preserving a prescribed bonded geometry to the rest of the system. In CONROT, the specific problem of reconfiguring an internal trimer of a molecule under the constraints of prescribed bond lengths and bond angles is solved.

Recently, Wu and Deem[21] proposed a more general methodology for the displacement of an internal part of a molecule through the implementation of inverse kinematics techniques developed in robotics for manipulations with the general spatial 7-link 7R mechanism. This formulation involves a module (mechanism) consisting of a sequence of seven pairs of vectors (joints and links). Every two successive vectors are perpendicular to each other and all together form a closed loop. With this configuration, it is possible to represent a manipulator in robotics or part of a chain molecule in atomistic simulation. The configuration of the chain molecular part is defined by six degrees of freedom and by six geometric constraints (bond lengths and bond angles), specifying how it is connected to the rest of the chain. The geometric problem solved by Wu and Deem is the following: "Given two atoms in a chain that are at least four rotatable bonds apart, find all possible configurations for the molecular segment in between the two atoms that satisfy the molecular constraints (bond lengths, bond angles, and any additional constraints)."

The molecular bridging methodology discussed above can be generalized to multiple chains, so that intramolecular as well as intermolecular bridging can occur. Depending on the position of the bridging part on the chain, one may have an end-bridging or an internal bridging move. Finally, a single bridge or a double bridge may be implemented, depending on the number of bridges that are formed simultaneously. In Figure 1, a schematic representation of various intramolecular and intermolecular bridging moves based on the concepts discussed here is shown. Obviously, a wealth of moves can be designed, depending on the system of interest and on the researcher's creativity.

In this work, two new bridging moves are introduced: the branch point slithering (BPS) and the branch point flip (BPF). All working equations are formulated in the semigrand canonical statistical ensemble, symbolized here by (N, n, P, T, $\boldsymbol{\mu}^*$), where N is the total number of chains in the system, n is the total number of atoms, P is the pressure, T the temperature, and $\boldsymbol{\mu}^*$

is a set of relative chemical potentials for all the chain species except two, which are taken as reference species.[13] The probability density function for this ensemble is

$$\rho^{NnPT\mu^*}(\mathbf{r}_1,\mathbf{r}_2,...,\mathbf{r}_n;\ \text{connectivity}) \propto \exp[\beta \sum_{\substack{k=1 \\ k\neq \text{ref chain} \\ \text{species}}}^{m} \mu_k^* N_k - \beta PV - \beta \mathcal{U}(\mathbf{r}_1,\mathbf{r}_2,...,\mathbf{r}_n;\ \text{connectivity})] \quad (1)$$

where $\mathbf{r}_i$ is the position vector of atom i, $\mathcal{U}$ is the potential energy function of the system, V is the volume, and $\beta = 1/(k_B T)$, with k_B being the Boltzmann constant.

The use of this ensemble is necessary in order to control the polydispersity of the system introduced by moves such as end-bridging.[13]

2.1. Acceptance Criteria. The starting point for the derivation of the acceptance criterion of a Monte Carlo move is the microscopic reversibility equation:[22]

$$a_{(o\to n)} A_{(o\to n)} P_{(o)} = a_{(n\to o)} A_{(n\to o)} P_{(n)} \quad (2)$$

where $a_{(i\to j)}$ is the conditional attempt probability of going from state i to state j, $A_{(i\to j)}$ is the conditional acceptance probability of going from state i to state j, and $P_{(i)}$ is the probability of the system being in state i. Subscripts o and n denote old and new states, respectively.

Conditional attempt probability $a_{(i\to j)}$ may include a number of bias selections to enhance subsequent acceptance of the move. The overall weight introduced due to this fact is

$$w_{(i\to j)} = \prod_{k=1}^{\text{no. of biased selections}} w'_{(i\to j),k}$$

where w' is the weight introduced from a single biased selection.

An appropriate Jacobian must be introduced to calculate $P_{(o)}$ and $P_{(n)}$ correctly when moving between different coordinate systems describing the phase space. If $\mathbf{q}$ is selected as the coordinate system, the a priori probability of the system being in state i is

$$P_i = \rho_i J_i \, d\mathbf{q} \quad (3)$$

where ρ_i is the normalized probability density function in Cartesian space determined by the statistical ensemble in use. Elementary volumes in Cartesian space and in $\mathbf{q}$-space around state i are related by $d\mathbf{r}_i = J_i \, d\mathbf{q}$.

The terms $a_{(i\to j)}$ are determined for the specific move. If the move consists of more than one independent steps, then the overall probability $a_{(i\to j)}$ as well as the Jacobian are calculated as products of the corresponding quantities for each step:

$$a_{(i\to j)} = \prod_{s=1}^{\text{no. of steps}} a_{(i\to j),s} \quad \text{and} \quad J_i = \prod_{s=1}^{\text{no. of steps}} J_{i,s} \quad (4)$$

From eqs 2−4, the generalized Metropolis acceptance criterion is obtained by imposing the condition of microscopic reversibility:

$$a_{(o\to n)} A_{(o\to n)} \rho_o J_o \, d\mathbf{q} = a_{(n\to o)} A_{(n\to o)} \rho_n J_n \, d\mathbf{q}$$

The acceptance probability is

$$A_{(o\to n)} = \min\left(1, \frac{\prod_{s=1}^{\text{no. of steps}} a_{(n\to o),s}\rho_n \prod_{s=1}^{\text{no. of steps}} J_{n,s}}{\prod_{s=1}^{\text{no. of steps}} a_{(o\to n),s}\rho_o \prod_{s=1}^{\text{no. of steps}} J_{o,s}}\right) \quad (5)$$

Equation 5 is further elucidated below for the two new elementary moves introduced here.

2.2. Branch Point Flip (BPF) and Branch Point Slithering (BPS). To relax the branch point of a chain molecule without the use of moves that alter drastically the connectivity of its atoms, two new moves are introduced here: the BPF and the BPS. Both moves are applicable to branch points with functionality 3.

During the BPF move, shown schematically in Figure 2, the branch point is flipped in one of three possible ways, corresponding to the three branches. Each way involves rotation about the axis defined by a pair of atoms adjacent to the branch point, keeping bond lengths fixed. In each case, the first atom of the third branch (i.e., the branch that does not contain any of the atoms in the axis pair) is reconstructed by selecting the two bond angles that define its position with respect to the branch point and the axis pair. Subsequently, a rebridge scheme is applied in order to reconnect that atom with the fifth atom of the third branch. In this way, the positions of the second through the fourth atom of the branch are changed. This procedure is called branch attachment scheme (BrAS). It should be noted that all derivations shown in this paper assume a constant bond length model for simplicity but remain equally valid for the case of flexible bond models. When flexible bond models are used, it is most convenient to perform a biased preselection of all bond lengths to be used in each move according to the Boltzmann factors of the corresponding bond stretching potentials.

Some important specifics of the move are described below.

• During the BrAS step the two bond angles that determine the position of the first atom of the third (moved) branch are selected according to the Boltzmann factor of the bending potential. From these angles two possible atom positions are calculated, one of which is selected at random. Thus, the weight introduced is

$$w_{\text{BrAS}(i\to j)} = \exp[-\beta \sum_{k=2,3} U_{\text{bend}}(\theta^j_{\text{bp},k})] \frac{1}{2} \quad (6)$$

where $\theta^j_{\text{bp},k}$ ($k = 2, 3$) are the bond angles $\theta_{\text{bp},2}$ and $\theta_{\text{bp},3}$ at the branch point (see Figure 3) in the j state.

• During the bridge step the five bond angles defining the trimer position are selected according to the Boltzmann factor of the bending potential. Subsequently, the solution s is selected among the possible bridging

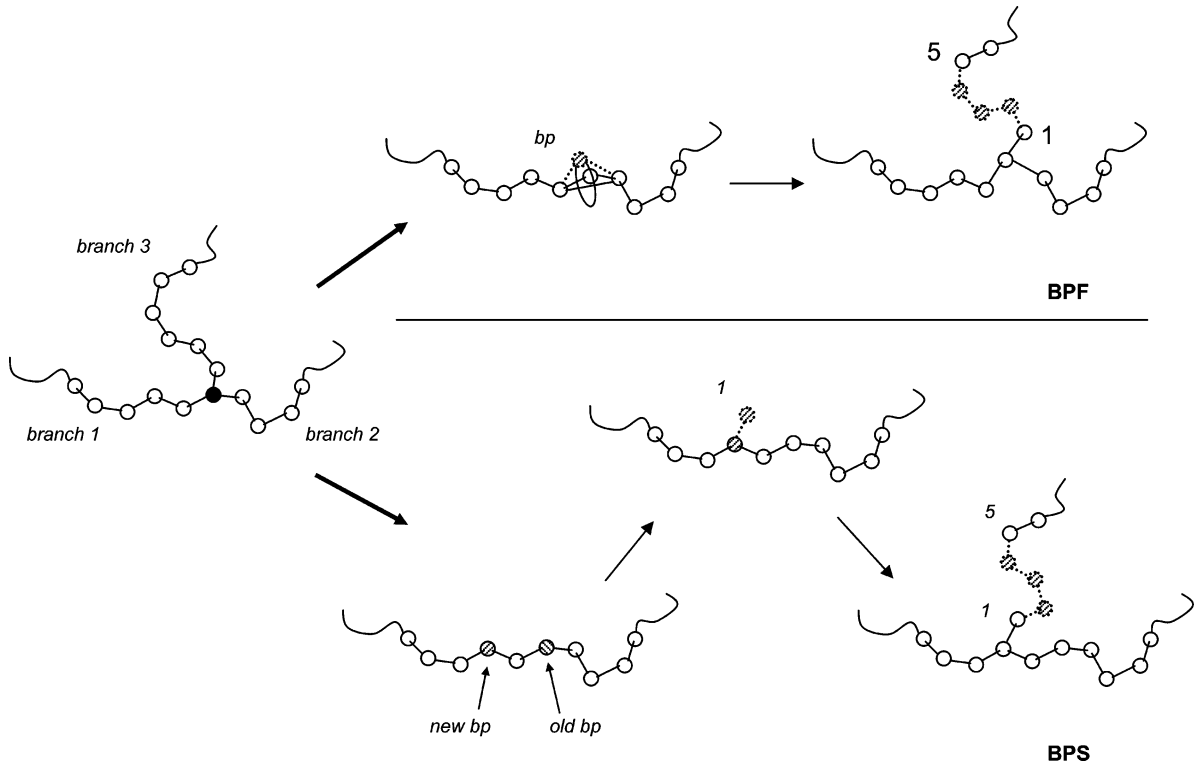

Figure 2. Schematic representation of the BPF (top) and BPS (bottom) moves.

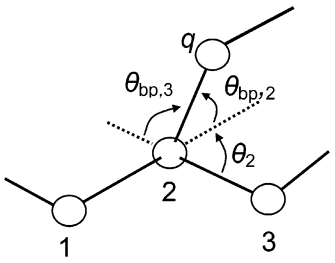

Figure 3. Detailed geometry for branch point (atom 2). During the slip step in BPF, atom 2 is rotated around the axis defined by atoms 1 and 3. Atom q is the first atom in the moved branch. A bond connecting atoms $i-1$ and i is denoted as bond i. The bond connecting atom q to the branch point is denoted as bond q.

solutions, based on the Boltzmann factor of the corresponding torsional energy:

$$w_{\text{bridge}(i\rightarrow j)} = \exp\left[-\beta\sum_{k=1}^{5}U_{\text{bend}}(\theta^{j}_{\text{br},k})\right] \frac{\exp\left[-\beta\sum_{k=1}^{6}U_{\text{tor}}(\phi^{j}_{\text{s},k})\right]}{\sum_{m=1}^{\text{no. of solutions}}\exp\left[-\beta\sum_{k=1}^{6}U_{\text{tor}}(\phi^{j}_{m,k})\right]} \quad (7)$$

where $\theta^{j}_{\text{br},k}$ is the bond angle k involved in the bridge leading to the j state, $\varphi^{j}_{m,k}$ is the torsion angle k of the m solution for the j state, and $\varphi^{j}_{s,k}$ denote the torsion angles of the selected solution.

For the flip step, a transformation of the coordinates of the flipped atom is considered:

$$\{\mathbf{r}_2\} \rightarrow \{b_2, b_3, \omega\} \quad (8)$$

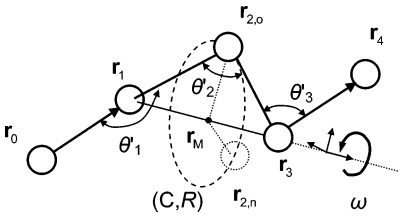

Figure 4. Schematic representation of the single flip move (where $\theta'_i = \pi - \theta_i$).

where ω is the rotational angle that controls the position of atom 2 on its locus [circle C defined by the fixed-length bonds 2 and 3, see Figures 3 and 4]. The corresponding Jacobian, J_F, depends only on the bond lengths b_2 and b_3 and the bond angle θ_2 of the moved atom, which are not changed (see Appendix A). Accordingly, the Jacobian is eliminated from the acceptance criterion.

To evaluate the Jacobian for the transformation of coordinates for the BrAS, that is $\{\mathbf{r}_q\} \rightarrow \{b_q, \theta_{\text{bp},2}, \theta_{\text{bp},3}\}$, the coordinates of the q atom (Figure 3) are expressed in the local Flory frame of the backbone bond $\mathbf{b}_3$, so that with the origin at the branch point

$$x'_q = -b_q\cos(\theta_{\text{bp},3})$$

$$y'_q = \frac{b_q}{\sin(\theta_2)}[\cos(\theta_{\text{bp},2}) + \cos(\theta_2)\cos(\theta_{\text{bp},3})]$$

$$z'_q = \pm\frac{b_q}{\sin(\theta_2)}[1 - \cos^2(\theta_2) - \cos^2(\theta_{\text{bp},2}) - \cos^2(\theta_{\text{bp},3}) - 2\cos(\theta_2)\cos(\theta_{\text{bp},2})\cos(\theta_{\text{bp},3})]^{1/2} \quad (9)$$

By applying straightforward trigonometric equations, one obtains

$$J_{\mathrm{BrAS}} = \left|\frac{\partial \mathbf{r}_q}{\partial(b_q,\theta_{\mathrm{bp},2},\theta_{\mathrm{bp},3})}\right|$$

$$= \frac{{b_q}^2 \sin(\theta_{\mathrm{bp},2}) \sin(\theta_{\mathrm{bp},3})}{[1 - \cos^2(\theta_2) - \cos^2(\theta_{\mathrm{bp},2}) - \cos^2(\theta_{\mathrm{bp},3}) - 2\cos(\theta_2)\cos(\theta_{\mathrm{bp},2})\cos(\theta_{\mathrm{bp},3})]^{1/2}} \quad (10)$$

If N_{bp}^i is the number of branch points of the system in state i, then the attempt probability for the BPF move is

$$a_{(i\to j)} = \frac{1}{N_{\mathrm{bp}}^i}\frac{1}{3} \quad (11)$$

because the branch point that participates in the move is randomly selected and there are three possible ways for flip.

Inserting eqs 6−11 in eq 5 and considering that the number of branch points in the system is constant, the acceptance criterion for BPF move becomes

$$A_{(\mathrm{o}\to\mathrm{n})} = \min\left(1, \frac{w_{\mathrm{BrAS(n\to o)}} w_{\mathrm{bridge(n\to o)}} \rho_{\mathrm{n}} J_{\mathrm{BrAS,n}} J_{\mathrm{Br,n}}}{w_{\mathrm{BrAS(o\to n)}} w_{\mathrm{bridge(o\to n)}} \rho_{\mathrm{o}} J_{\mathrm{BrAS,o}} J_{\mathrm{Br,o}}}\right) \quad (12)$$

where J_{Br} is the Jacobian for the bridge step. J_{Br} is a quite lengthy expression and can be found elsewhere.[13,15,20,23]

The BPS move was developed on the basis of the concept that a branch point can slither along the "backbone" defined by any two of the branches attached to it (see Figure 2). Slithering of the branch point is constrained by the molecular weight distribution of the branches. Once the branch point is displaced, the third branch is reconnected to the backbone using the BrAS. The first atom of the branch is constructed by using the corresponding bond length and the two bond angles. Relaxation of the atoms in the vicinity of the branch point is achieved using standard moves such as flip, DF, and CONROT.

The attempt probability for the BPS move is equal to

$$a_{(i\to j)} = \frac{1}{N_{\mathrm{bp}}^i}\frac{1}{3}\frac{1}{2}\frac{1}{n_s} \quad (13)$$

where n_s is the number of positions (atoms) to which the branch point is allowed to move in each direction along the "backbone" of the molecule. Equation 13 accounts for the random selection performed with respect to (a) the branch point that is going to participate in the move, (b) the different branches adjacent to a given branch point, (c) the direction of slithering, and (d) n_s (here, $n_s = 1$ or 2). The acceptance criterion for BPS is the same with that of the BPF move, given in eq 12.

2.3. Dimer Flip (DF). The DF move is an extension of the simple flip move.[11] Development of this move is motivated by the need for a larger number of fluctuating degrees of freedom during a single move. The flip move can be extended further to n atoms, so that reconnection of segments of the same or different chains within a force field using flexible bond angles can be achieved.

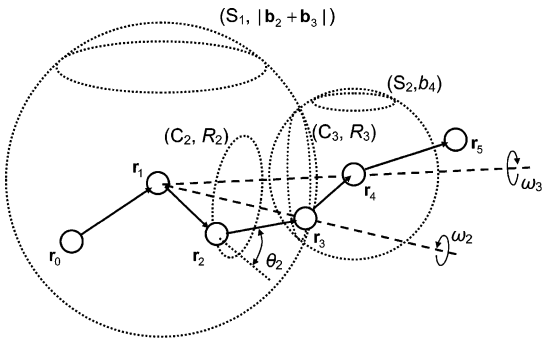

Figure 5. Schematic representation of the DF move. The atoms that are displaced are 2 and 3.

In Figure 5, the DF move is illustrated schematically. The position of atom 3 is altered by changing torsional angle ω_3 that defines the atom position on the circle C_3, which constitutes the intersection of a sphere S_1 centered at $\mathbf{r}_1$ with radius $|\mathbf{b}_2 + \mathbf{b}_3|$ and sphere S_2 centered at $\mathbf{r}_4$, of radius b_4. Note that during the DF construction the distance l_{13} between atoms 1 and 3 and bond length b_4 are kept equal to their old values. Once the position of atom 3 has been fixed, the position of atom 2 is changed by applying a simple flip move (i.e., by changing angle ω_2 that defines the position of atom 2 on the circle C_2, which is the locus of this atom for given bond lengths b_2 and b_3). In the implementation of the move, a transformation is performed from the Cartesian coordinates of the dimer to a set of variables attached to the dimer: $\{\mathbf{r}_2,\mathbf{r}_3\} \rightarrow \{b_2,b_3,\omega_2,l_{13},b_4,\omega_3\}$. For this reason, a Jacobian is introduced in the acceptance criterion of the move:

$$J_{\mathrm{DF}} = \frac{\partial(\mathbf{r}_2,\mathbf{r}_3)}{\partial(b_2,b_3,\omega_2,l_{13},b_4,\omega_3)} \quad (14)$$

The evaluation of the Jacobian is given in Appendix B. The acceptance criterion is calculated easily from eqs 1 and 5, taking into account that no bias weights are introduced in the move:

$$A_{(\mathrm{o}\to\mathrm{n})} = \min\left(1, \frac{a_{(\mathrm{n}\to\mathrm{o})}\rho_{\mathrm{n}} J_{\mathrm{DF,n}}}{a_{(\mathrm{o}\to\mathrm{n})}\rho_{\mathrm{o}} J_{\mathrm{DF,o}}}\right) \quad (15)$$

with

$$a_{(i\to j)} = \frac{1}{N_{\mathrm{ch}} n_{\mathrm{ch,DF}}} \quad (16)$$

where N_{ch} is the number of chains in the system and $n_{\mathrm{ch,DF}}$ is the number of atoms of the selected chain that can participate in the move.

The n-mer flip move can be performed by applying the following methodology for atom i, $i = 2, \ldots, n + 1$: Given the positions of atoms 1 ($\mathbf{r}_1$) and $i + 1$ ($\mathbf{r}_{i+1}$) and the distances $|\mathbf{r}_i - \mathbf{r}_1|$ and $|\mathbf{r}_{i+1} - \mathbf{r}_i|$, atom i is displaced on the periphery of the circle C_i which is the locus of positions for atom i given the constraints imposed by the molecular architecture. This displacement is brought about by changing the rotational degree of freedom ω_i.

3. Simulation Details

In this work, melts of symmetric triarm star polyethylene chains of various lengths were simulated. The mean arm lengths examined were 40, 100, and 200 carbon atoms. The numbers of chains in the simulation

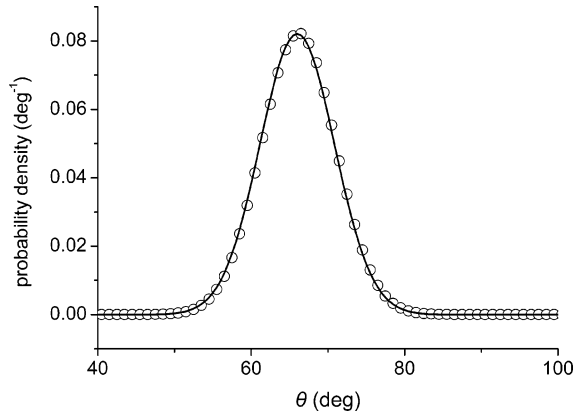

Figure 6. Normalized distribution of the bond angle centered at the $-CH_2-$ UA for a linear phantom chain C_{60} at 450 K. The run size was 2×10^6 moves, and the moves used were 2% reptation and 98% DF. The solid line corresponds to the theoretical distribution based on the force field, and the points are simulation results.

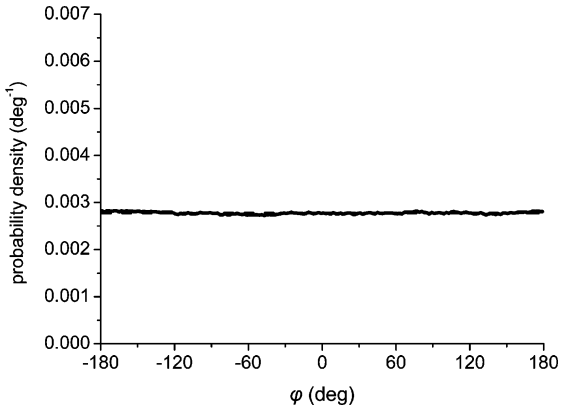

Figure 7. Normalized distribution of the torsional angle around the $-CH_2-CH_2-$ bond for a linear phantom chain C_{60} at 450 K. The run size was 2×10^6 moves, and the moves used were 2% reptation and 98% DF. The dashed line corresponds to the ideal uniform distribution, and the solid line is the simulation results (the two lines practically coincide).

box were 16, 6, and 4, respectively. In all cases, the pressure was set equal to 0.1 MPa, whereas various temperature values were examined. A typical Monte Carlo simulation run consisted of the following moves: 6% reptation, 3% rotation, 3% DF, 20.5% CONROT, 43% end-bridge, 0.5% volume fluctuation, 12% BPF, and 12% BPS. For the PVT properties simulations were performed at 450, 475, 500, 525, and 550 K and 0.1 MPa. In this case the move blend consisted of 6% reptation, 3% rotation, 3% DF, 20.5% CONROT, 41.5% end-bridge, 2% volume fluctuation, 12% BPF, and 12% BPS. All runs were performed on AMD Athlon MP 1800+ processors. For comparison, MC simulations of linear polyethylene were also performed.

In all cases the force field employed was TraPPE, an accurate united atom (UA) force field developed for thermodynamic properties of linear and branched alkanes and later extended to other classes of organic compounds.[18,24] In TraPPE bond lengths are kept constant, whereas bond angle bending and dihedral angle torsions are calculated using appropriate expressions. Finally, nonbonded intra- and intermolecular interactions are calculated from the Lennard-Jones potential with parameters fitted to saturated liquid density and vapor pressure experimental data.

For nonbonded interactions the Lennard-Jones potential was truncated at $r = 2.5\sigma$ for all types of interactions. The branch molecular weight (bMW) distribution was uniform in the interval $[\bar{X}(1 - \Delta), \bar{X}(1 + \Delta)]$ with $\Delta = 0.5$ and $\bar{X}$ the mean bMW. The relative chemical potential was set equal to zero for all the branches that satisfy the bMW distribution and minus infinity in all other cases.

4. Results and Discussion

4.1. Structural Characteristics. To test that DF was properly implemented in the MC code, a linear C_{60} phantom chain (that is a chain with only bond angle bending interactions) was simulated at 450 K. The MC simulation consisted of 2×10^6 moves with 2% reptation and 98% DF, only. These moves alter both the bond angles and the torsional angles.

The normalized distribution of the bond angles, as obtained from the linear phantom chain simulations, is shown in Figure 6. For comparison, the theoretical distribution ($\propto \sin(\theta)\ \exp[-\beta U_{\text{bend}}(\theta)]$) calculated from the TraPPE force field is plotted. The two sets of calculations coincide over the entire spectrum of bond angle values. Furthermore, the normalized distribution of torsion angles in the linear phantom chain is shown in Figure 7 together with the theoretically expected uniform distribution. In a phantom chain, all torsion angle values are equally probable. Indeed, the moves used do not impose any bias in the torsion angle distribution; this provides a strong indication that the moves have been implemented properly.

The proper implementation of the two new moves for the branch point, that is BPF and BPS, was evaluated through the simulation of a symmetric triarm C_{60} phantom chain (three arms of 20 UA each) at 450 and 500 K. In this case, the run consisted of 2×10^6 MC moves composed of 2% reptation, 10% CONROT, 44% BPF, and 44% BPS.

From eq 10 it is clear that the bond angles around a branch point (triad) are coupled. In the case of a phantom chain, the probability for the bond angle triad is given by the equation

$$P(\theta_2,\theta_{\text{bp},2},\theta_{\text{bp},3}) \propto \exp[-\beta U_{\text{bend}}(\theta_2)] \prod_{i=2}^{3} \exp[-\beta U_{\text{bend}}(\theta_{\text{bp},i})]\ \mathrm{d}\mathbf{r}_3\, \mathrm{d}\mathbf{r}_q \quad (17)$$

with the angles θ_2, $\theta_{\text{bp},2}$, and $\theta_{\text{bp},3}$ being functions of the coordinates of atoms 3 and q (Figure 3). Upon application of the trivial transformation from the Cartesian coordinates of atom 3 to the Flory coordinates[25] (b_3, θ_2, φ_2), with φ_2 being the dihedral angle of atoms 0, 1, 2, and 3, the equation above yields

$$P(\theta_2,\theta_{\text{bp},2},\theta_{\text{bp},3}) \propto \exp[-\beta U_{\text{bend}}(\theta_2)] \prod_{i=2}^{3} \exp[-\beta U_{\text{bend}}(\theta_{\text{bp},i})] J_{\text{Flory}} J_{\text{BrAS}}\, \mathrm{d}\phi_2\, \mathrm{d}\theta_2\, \mathrm{d}\theta_{\text{bp},2}\, \mathrm{d}\theta_{\text{bp},3} \quad (18)$$

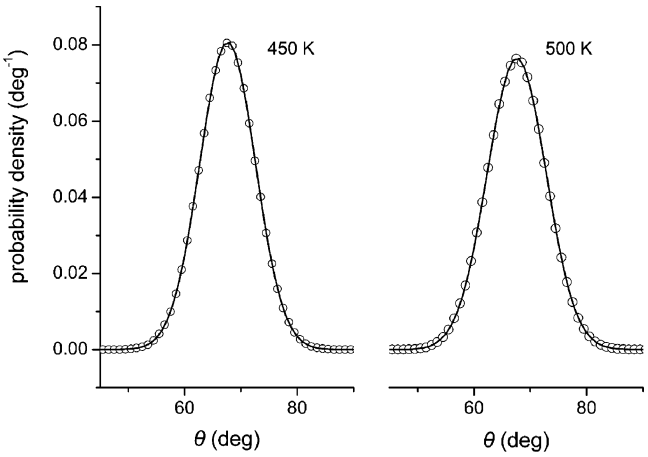

Figure 8. Collective normalized distribution of the three bond angles around the branch point for a symmetric triarm star C_{60} phantom chain (three arms of 20 UA each) at 450 and 500 K. The solid line corresponds to the distribution based on eq 20, and the points are simulation results.

with $J_{\text{Flory}} = \partial(\mathbf{r}_3)/\partial(b_3,\theta_2,\varphi_2) = {b_3}^2 \sin(\theta_2)$ being the Jacobian of transformation to Flory coordinates. Substituting eq 10 in eq 18, we finally obtain

$$P(\theta_2,\theta_{\text{bp},2},\theta_{\text{bp},3}) \propto 2\pi {b_3}^2 {b_q}^2 \exp[-\beta U_{\text{bend}}(\theta_2)] \prod_{i=2}^{3} \exp[-\beta U_{\text{bend}}(\theta_{\text{bp},i})] \sin(\theta_2) \sin(\theta_{\text{bp},2}) \sin(\theta_{\text{bp},3}) \Big/ [1 - \cos^2(\theta_2) - \cos^2(\theta_{\text{bp},2}) - \cos^2(\theta_{\text{bp},3}) - 2\cos(\theta_2)\cos(\theta_{\text{bp},2})\cos(\theta_{\text{bp},3})]^{1/2} \, \mathrm{d}\theta_2 \, \mathrm{d}\theta_{\text{bp},2} \, \mathrm{d}\theta_{\text{bp},3} \quad (19)$$

This equation is symmetric with respect to the three bond angles, as expected. The probability distribution ρ for each of the bond angles is given by the equation

$$\rho(\theta_2) = \frac{\int_0^\pi \mathrm{d}\theta_{\text{bp},2} \int_0^\pi \mathrm{d}\theta_{\text{bp},3} P(\theta_2,\theta_{\text{bp},2},\theta_{\text{bp},3})}{\int_0^\pi \mathrm{d}\theta_2 \int_0^\pi \mathrm{d}\theta_{\text{bp},2} \int_0^\pi \mathrm{d}\theta_{\text{bp},3} P(\theta_2,\theta_{\text{bp},2},\theta_{\text{bp},3})} \quad (20)$$

In Figure 8, the collective normalized distribution of the three bond angles around the branch point is shown at two temperatures, together with the theoretical distribution calculated from the TraPPE force field for branched hydrocarbons[18] using eqs 19 and 20. In both cases, the two sets of calculations coincide. In Figure 9, the collective normalized distribution of the three torsional angles around the ⟩CH−CH$_2$− bonds is shown for the same system at 450 K. The probability density is constant, independent of the torsional angle value, as expected for a phantom chain. This provides a strong indication that both BPF and BPS are implemented properly with respect to molecular architecture constraints.

MC simulations in the (N, n, P, T, $\boldsymbol{\mu}^*$) ensemble were performed on melts of symmetric triarm star C_{600} chains, of mean molar mass 8402 g mol^{-1}. The temperature was set equal to 450 K and the pressure to 0.1 MPa. A total number of 5×10^7 MC moves were attempted. The blend of the moves was discussed in the simulation details section. In Table 1, the acceptance ratio for the various moves is shown. With the exception of the end-bridging move (EB), all other moves exhibit

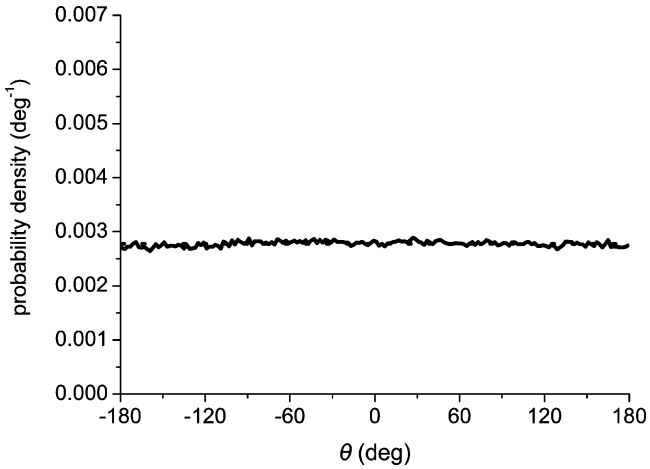

Figure 9. Normalized distribution of the torsional angles around the ⟩CH−CH$_2$− bonds for a triarm C_{60} phantom chain (three arms with 20 UA each) at 450 K. The dashed line corresponds to the uniform ideal distribution, and the solid line is the simulation data (the two lines practically coincide).

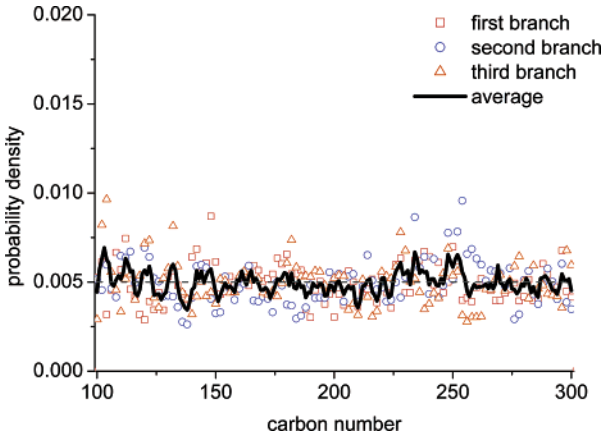

Figure 10. Probability distribution of the size of each of the three branches and of their average in a melt of triarm symmetric C_{600} star chains with $\Delta = 0.5$ at 450 K and 0.1 MPa from a MC simulation of 5×10^7 moves.

Table 1. Percentage Acceptance of MC Moves for Triarm Symmetric Star C_{120}, C_{300}, and C_{600} Chain Melts at 450 K and 0.1 MPa

carbon no.	REP	ROT	FLIP	CONROT	EB	VOL	DF	BPS	BPF
120	7.0	18.1	77.8	9.5	0.2	10.2	67.2	1.1	3.8
300	6.9	17.3	78.1	8.9	0.2	8.0	67.3	1.2	3.9
600	8.0	18.2	78.3	8.5	0.2	5.6	67.1	0.9	4.0

significant acceptance ratios. Interestingly, the DF move has only 10% lower acceptance than the simple flip move and so should be preferred over the simple flip, since it allows simultaneous rearrangement of two atoms instead of only one. For comparison, the acceptance ratio is shown for MC simulations of melts of symmetric triarm chains of smaller length (C_{120} and C_{300}) at the same conditions. No significant change is observed with respect to the size of the chain molecules examined.

The ability of the elementary moves utilized to provide uniform sampling of all branch lengths allowed, based on the chemical potential values imposed, is assessed in Figure 10. The mean carbon number per branch is 200 and $\Delta = 0.5$, so that the allowable branch size is between 100 and 300 carbon numbers. The distribution of the size of each branch is shown, together with the average distribution over all three branches. In all cases, all branch sizes exhibit the same probability

$$P_{(n)} = \begin{cases} 0 & \text{for} \quad n < 3a \\ \dfrac{(n-3a+2)(n-3a+1)}{2(b-a+1)^3} & \text{for} \quad 3a \le n \le 2a+b \\ \dfrac{(n-3a+2)(n-3a+1)-3(n-2a-b+1)(n-2a-b)}{2(b-a+1)^3} & \text{for} \quad 2a+b < n \le a+2b \\ \dfrac{(3b-n+2)(3b-n+1)}{2(b-a+1)^3} & \text{for} \quad a+2b < n \le 3b \\ 0 & \text{for} \quad n > 3b \end{cases} \tag{21}$$

density (within a statistical uncertainty), and the elementary moves utilized result in uniform sampling of the branch length. The probability distribution for the average size (number of carbons) of the tristar chain can be derived easily from the branch distributions. The sum, n, of three integer random variables distributed uniformly in the interval $[a, b]$ (corresponding to the three branches) is governed by the probability density function (eq 21).

The shape of this distribution is already close to a Gaussian. (It would be expected to become Gaussian for stars of many arms.) In our case, n is the number of atoms of the chain and a, b are the lower and upper bounds in the uniform distribution of each branch.

The probability distribution of the total chain size in our simulated symmetric triarm C_{120} star melt is depicted in Figure 11a. In the same figure, the analytical distribution calculated from eq 21 and a Gaussian fit to the simulation data are shown. The good agreement between the theoretical curve and the simulation results confirms that the molecular weight distribution can be fully controlled in our triarm star melt simulation. In the case of C_{600} (Figure 11b), a noticeable difference is observed between the Gaussian fit and the analytical distribution. The reason for this is the size of the system (the simulation box contains only four chains in the latter case). Very long and very short chains are more active as victims or attackers during the end-bridging move, so their residence time in the system is short. Hence, the calculated distribution (for the branches and consequently for the chains) is augmented near the mean value and diminished at the edges. To verify this, a simulation was performed in an ideal system of phantom branched chains (absence of any kind of inter- and intramolecular interactions) where random mixing occurs (each end can attack all the atoms of all the other chains). As shown in Figure 12a,b, as the number of chains increases, the calculated branch length and chain length distributions coincide with the "expected" distributions. Interestingly, for the same number of chains, the distributions calculated from the ideal and the "real" system are nearly the same.

It is well-known, both experimentally and theoretically, that the squared radius of gyration (R_G) of a polymer melt varies linearly with the molecular weight.[25] Our MC simulation results for the triarm C_{600} with $\Delta = 0.5$ follow this trend, as shown in Figure 13. It should be noted that chains of very low (for carbon number between 300 and 450) and of very high (for carbon number between 750 and 900) size are not sampled adequately during the simulation, and so there is considerable scatter from the overall trend. Results for these low and high ends in the spectrum of chain size are shown as points in Figure 13.

Furthermore, the size of individual arms has been calculated as a function of arm length. In Figure 14,

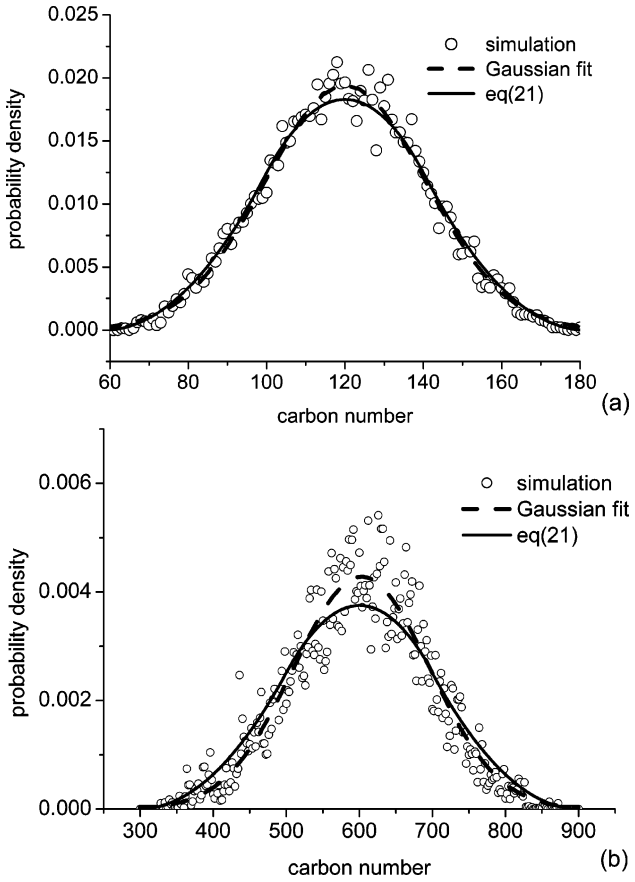

Figure 11. Probability distribution of the chain size. (a) In a melt of C_{120} triarm star chains with $\Delta = 0.5$ at 450 K and 0.1 MPa from MC simulation (points). The Gaussian fit is of the form $(1/\sqrt{2\pi}\sigma)\exp[-(n-\bar{n})^2/2\sigma^2]$, with $\bar{n} \sim 120$ and $\sigma \sim 20.6$. The solid line displays the analytical distribution, eq 21, plotted with $a = 20$ and $b = 60$. (b) In a melt of C_{600} triarm star chains with $\Delta = 0.5$ at 450 K and 0.1 MPa from MC simulation (points). The Gaussian fit is of the form $(1/\sqrt{2\pi}\sigma)\exp[-(n-\bar{n})^2/2\sigma^2]$, with $\bar{n} \sim 603$ and $\sigma \sim 93.2$. The solid line displays the analytical distribution, eq 21, plotted with $a = 100$ and $b = 300$.

the mean-squared distance from the arm end to the branch point, normalized with respect to the squared bond length, is shown as a function of the arm carbon number for the three arms of the triarm star polymer. In all cases, the mean-squared arm size is a linear function of the carbon number (within statistical uncertainty).

The pair radial distribution functions of the triarm symmetric polymers under examination at 450 K and 0.1 MPa are shown in Figure 15. In all cases, $g(r)$ for the CH_3-CH_2 pair exhibits a much higher peak than $g(r)$ for the CH_2-CH_2 pair. This is due to the Lennard-Jones energy parameter values used in TraPPE: $\epsilon_{CH_3-CH_2}/k_B = 67.1$ K while $\epsilon_{CH_2-CH_2}/k_B = 46$ K, and so the former

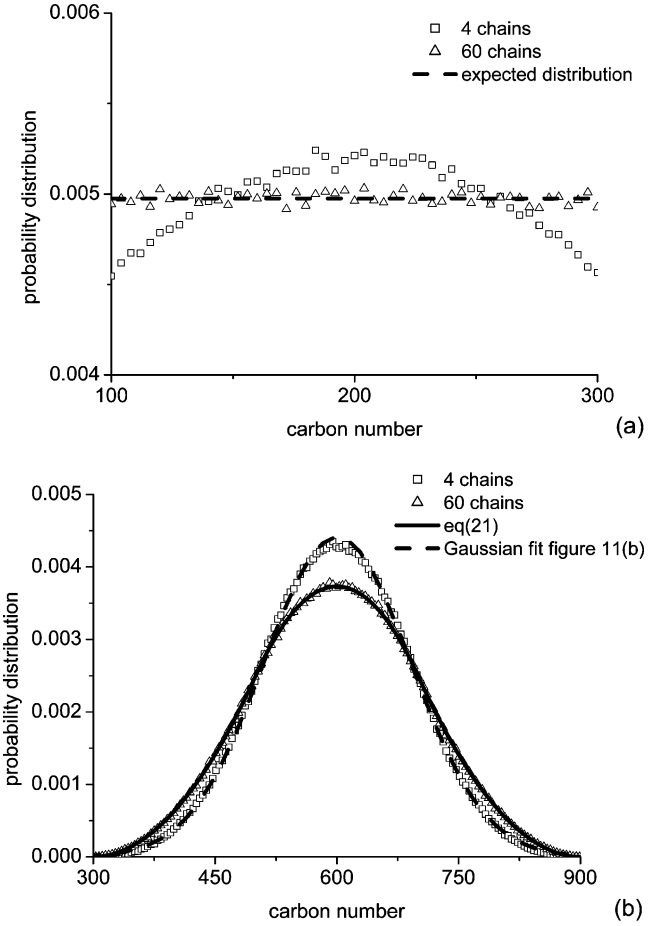

Figure 12. (a) Branch length and (b) chain size distributions for an ideal system of branched chains (C_{600}), where the random mixing assumption holds. As the number of chains of the system increases, the calculated distribution approaches the "expected" distribution.

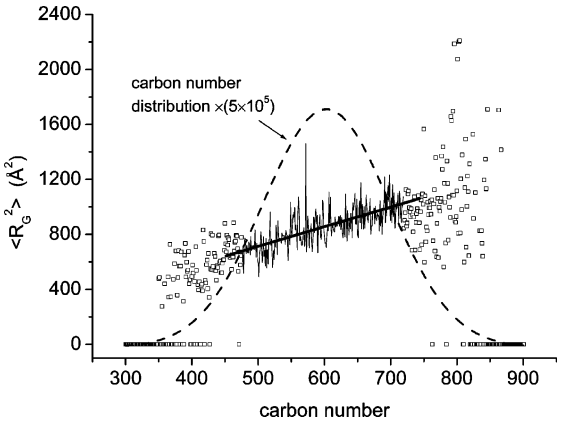

Figure 13. Chain squared radius of gyration as a function of carbon number for a triarm C_{600} system at 450 K and 0.1 MPa. In the lower (300−450) and higher (750−900) regions of carbon numbers the statistics is very poor, and results are shown as points.

pair of UAs is more attractive than the latter. For comparison, the same pair radial distribution functions for the cases of linear analogues at the same conditions are included in the figure. Interestingly, $g_{CH_3-CH_2}(r)$ for the linear and branched polymers are similar, whereas $g_{CH_2-CH_2}(r)$ is consistently higher for the linear polymer than for the corresponding triarm star polymer. The difference in $g_{CH_2-CH_2}(r)$ between the two polymers reflects the fact that the triarm macromolecules are more compact (denser) objects than linear chains of the same molecular weight. As a consequence, they exhibit a stronger "correlation hole" effect[11,15] in the melt. This effect becomes stronger with the increase of the MW of the polymer chain. In the case of C_{600} the "correlation hole" effect is noticeable even for the CH_3-CH_2 pair.

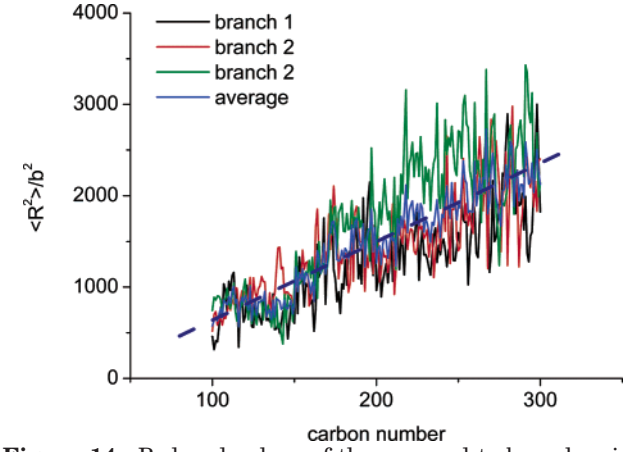

Figure 14. Reduced values of the arm end to branch point distance for the three branches and their average for a triarm C_{600} system at 450 K and 0.1 MPa. The dashed line is the linear fit to the average.

4.2. Chain Relaxation. An important consideration for the elementary moves introduced here is whether they are able to relax long chain molecules efficiently. Some of the MC moves most widely used today, such as configurational bias, CONROT, EB, DB etc., were developed primarily to address this problem.[8−14] In Figure 16, the autocorrelation functions for three characteristic vectors of a triarm symmetric C_{600} chain are presented. An autocorrelation function is defined according to the product $\langle \hat{\mathbf{v}}_0 \cdot \hat{\mathbf{v}}_i \rangle$, where $\hat{\mathbf{v}}_0$ and $\hat{\mathbf{v}}_i$ are the unit vectors along a section of the chain at the beginning of the simulation and after a certain number i of MC moves. The different vectors recorded in the simulation that characterize the geometry of the triarm chain or part thereof are (a) the branch point vector, $\hat{\mathbf{v}}_{bp}$, that is the unit vector along the vectorial sum of the three bonds converging at the branch point (with reference to Figure 3: $\hat{\mathbf{v}}_{bp} = (\mathbf{r}_{2,q} + \mathbf{r}_{2,1} + \mathbf{r}_{2,3})/|\mathbf{r}_{2,q} + \mathbf{r}_{2,1} + \mathbf{r}_{2,3}|$, (b) the arm end-to-branch point unit vector, $\hat{\mathbf{v}}_{eb}$, and (c) the arm end-to-arm end unit vector, $\hat{\mathbf{v}}_{ee}$.

Calculations presented in Figure 16 indicate clearly that all three autocorrelation functions decay to zero relatively fast, thanks to the MC moves used for this system. The branch point vector seems to relax faster, which indicates the efficiency of the new moves introduced here specifically for this purpose. In Figure 17, relaxation of $\hat{\mathbf{v}}_{bp}$ is shown for triarm chains of variable size (C_{120}, C_{300}, and C_{600}) and also for the C_{600} triarm chain from a MC simulation without the use of BPS and BPF. In the latter case the relaxation is considerably slower, indicating the efficiency of the new moves in relaxing the branch point and its neighboring atoms. The new moves relax equally fast all the chain sizes examined.

4.3. Volumetric Properties of Linear and Triarm Star Polyolefins. The last section of this paper is devoted to the melt density of the triarm star polymer for different molecular sizes and its temperature dependence. In Figure 18, MC simulation results are presented for the mass density of the triarm symmetric star C_{300} polymer and its corresponding linear polymer at various temperatures and 0.1 MPa. Experimental

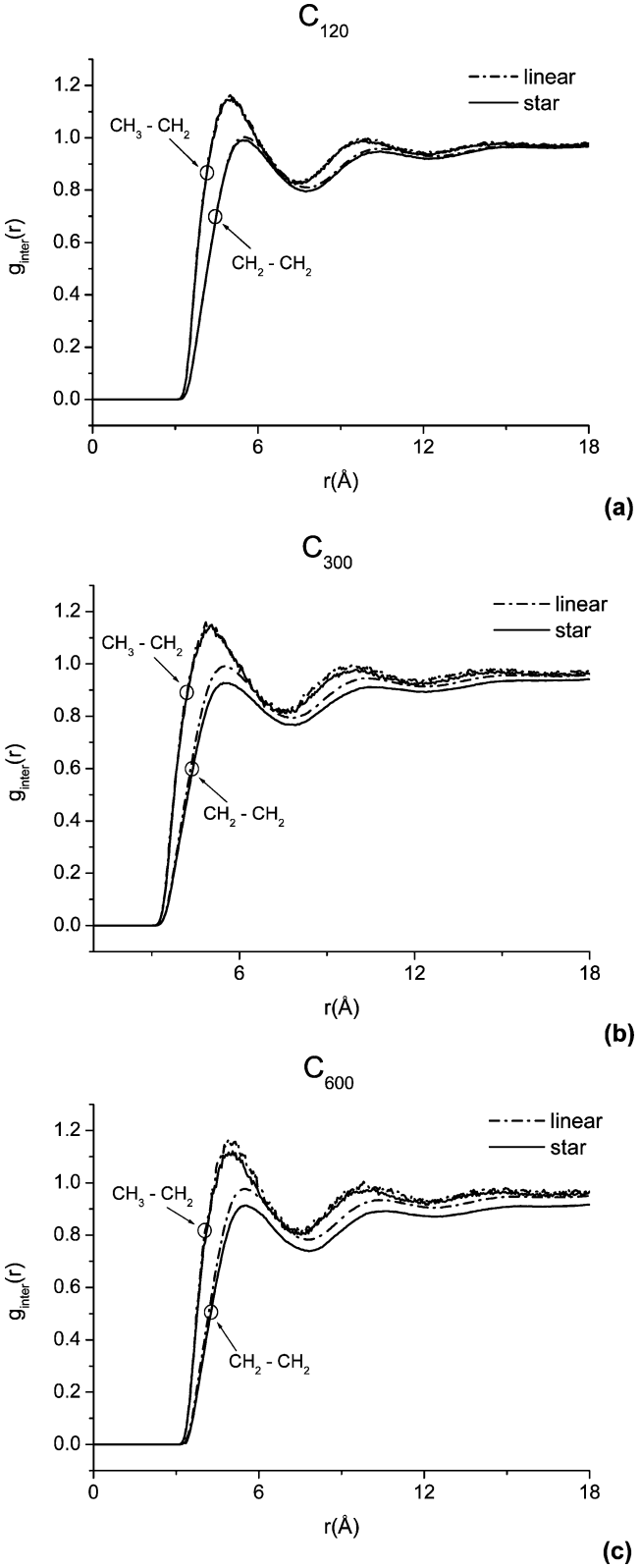

Figure 15. Pair radial distribution functions for (a) the linear C_{120} and triarm C_{120} (3×40) polymers (sixteen chains), (b) the linear C_{300} and triarm C_{300} (3×100) polymers (six chains), and (c) the linear C_{600} and triarm C_{600} (3×200) polymers (four chains), at 450 K and 0.1 MPa. In all cases the run length was 5×10^7 moves. Curves were generated from 1000 configurations evenly distributed throughout the run.

data[26] for high-density polyethylene (linear) and low-density polyethylene (branched) are shown for comparison. At all temperatures, the melt density of the linear polymer is higher than that of the triarm polymer.

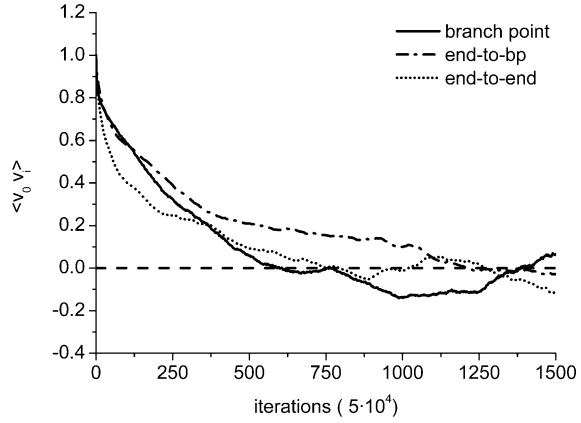

Figure 16. Relaxation of the characteristic vectors of symmetric triarm star C_{600} (3×200) chains in a melt at 450 K and 0.1 MPa. Simulation was performed on an Athlon MP1800+ for a total duration of 1.4×10^5 CPU s.

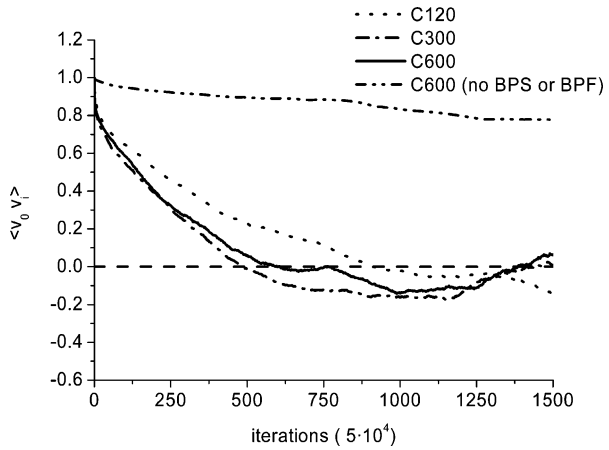

Figure 17. Relaxation of the branch point characteristic vector, $\hat{\mathbf{v}}_{bp}$, of triarm star chain melts of variable chain size (C_{120}, C_{300}, C_{600}) at 450 K and 0.1 MPa. Results for triarm star C_{600} are also shown from a MC simulation with the following distribution of moves: 10% reptation, 6% rotation, 6% flip, 25.5% CONROT, 52% end-bridging, 0.5% volume fluctuation.

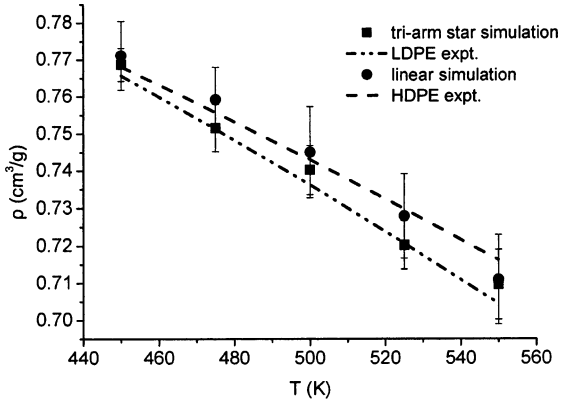

Figure 18. Melt density of triarm C_{300} and linear C_{300} at 450, 475, 500, 525, and 550 K and 0.1 MPa from MC simulation. Experimental data[26] for HDPE and LDPE are shown for comparison.

Furthermore, MC simulation predictions for the linear polyethylene agree well with the HDPE data, while simulation predictions for the triarm star polyethylene agree well with the LDPE data. It is concluded that TraPPE is an accurate force field for density predictions of polyolefins of variable architecture.

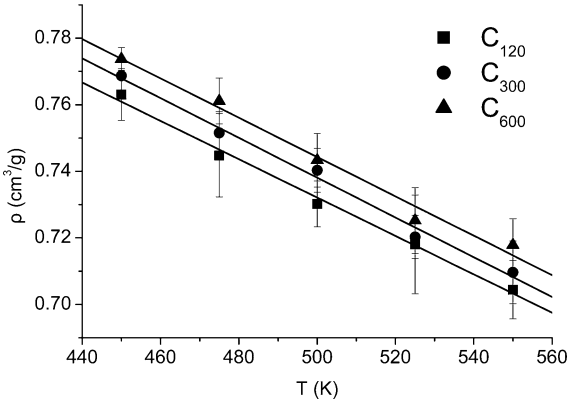

Figure 19. Melt density of triarm C_{120}, C_{300}, and C_{600} at 450, 475, 500, 525, and 550 K and 0.1 MPa from MC simulation. The solid lines are fit to the simulation results and are drawn to guide the eye.

Finally, in Figure 19 a comparison is shown for the melt density of triarm star polyethylenes of different molecular sizes, namely C_{120}, C_{300}, and C_{600}, as predicted from MC simulation. As one might expect, melt density increases with increasing molecular weight at constant temperature and pressure.

5. Conclusions

In this work novel elementary MC moves for the simulation of chain molecules were developed. The moves focus specifically on the efficient equilibration of branch point(s). It was shown that these moves result in efficient relaxation of systems of triarm star chain molecules of considerable molecular weight. A combination of existing and new moves was used for the calculation of structure and thermodynamic properties of triarm star polyethylene. This work focused entirely on pure polymers. In a future publication, mixtures of linear and branched polyolefins will be examined, aiming at an understanding of molecular aspects of polymer blend miscibility.

Acknowledgment. Financial support for this work provided by the General Secretariat of Research and Technology, Greece, through the PENED99 program to I.G.E. is gratefully acknowledged. The CINECA Supercomputer Center in Bologna, Italy, is acknowledged for a visiting post-graduate fellowship and generous allocation of supercomputing time to L.D.P. through the MINOS program.

Appendix A. Jacobian for the Flip Move

The Jacobian of the flip move transformation, eq 8, is

$$J_F = \frac{\partial(\mathbf{r}_2)}{\partial(b_2,b_3,\omega)} \tag{A.1}$$

To calculate J_F, the following partial derivatives need to be calculated:

$$\frac{\partial \mathbf{r}_2}{\partial b_2} = \frac{\partial(\mathbf{r}_2 - \mathbf{r}_1)}{\partial b_2} = \frac{\partial \mathbf{b}_2}{\partial b_2} = \frac{\partial(b_2\hat{\mathbf{u}}_2)}{\partial b_2} = \hat{\mathbf{u}}_2 \tag{A.2}$$

$$\frac{\partial \mathbf{r}_2}{\partial b_3} = -\frac{\partial(\mathbf{r}_3 - \mathbf{r}_2)}{\partial b_3} = -\frac{\partial \mathbf{b}_3}{\partial b_3} = -\frac{\partial(b_3\hat{\mathbf{u}}_3)}{\partial b_3} = -\hat{\mathbf{u}}_3 \tag{A.3}$$

$$\frac{\partial \mathbf{r}_2}{\partial \omega} = \frac{\partial(\mathbf{r}_2 - \mathbf{r}_1)}{\partial \omega} = \frac{\partial \mathbf{b}_2}{\partial \omega} = \frac{(\mathbf{r}_3 - \mathbf{r}_1) \times \mathbf{b}_2}{|(\mathbf{r}_3 - \mathbf{r}_1) \times \mathbf{b}_2|} R \tag{A.4}$$

where R is the radius of circle C (Figure 4) and $\hat{\mathbf{u}}_i$ stands for the unit vector along bond $\mathbf{b}_i$.

Knowing that

$$(\mathbf{r}_3 - \mathbf{r}_1) \times \mathbf{b}_2 = (\mathbf{b}_2 + \mathbf{b}_3) \times \mathbf{b}_2 = \mathbf{b}_3 \times \mathbf{b}_2 \tag{A.5}$$

$$|\mathbf{b}_3 \times \mathbf{b}_2| = |(\mathbf{r}_3 - \mathbf{r}_1)|R \tag{A.6}$$

eq A.4 results in

$$\frac{\partial \mathbf{r}_2}{\partial \omega} = \frac{\mathbf{b}_3 \times \mathbf{b}_2}{|(\mathbf{r}_3 - \mathbf{r}_1)|} = b_2 b_3 \frac{\hat{\mathbf{u}}_3 \times \hat{\mathbf{u}}_2}{|(\mathbf{r}_3 - \mathbf{r}_1)|} \tag{A.7}$$

Substituting eqs A.2, A.3, and A.7 in eq A.1, the Jacobian of the flip move is finally obtained:

$$J_F = \left|\begin{vmatrix} \hat{\mathbf{u}}_2^{\mathrm{T}} & -\hat{\mathbf{u}}_3^{\mathrm{T}} \end{vmatrix} \begin{pmatrix} b_2 b_3 \frac{\hat{\mathbf{u}}_3 \times \hat{\mathbf{u}}_2}{|(\mathbf{r}_3 - \mathbf{r}_1)|} \end{pmatrix}^{\mathrm{T}} \right| =$$

$$\frac{b_2 b_3}{|(\mathbf{r}_3 - \mathbf{r}_1)|} \left| \begin{vmatrix} \hat{\mathbf{u}}_2 \\ \hat{\mathbf{u}}_3 \\ \hat{\mathbf{u}}_3 \times \hat{\mathbf{u}}_2 \end{vmatrix} \right| =$$

$$\frac{b_2 b_3}{|(\mathbf{r}_3 - \mathbf{r}_1)|} |[\hat{\mathbf{u}}_2 \cdot (\hat{\mathbf{u}}_3 \times (\hat{\mathbf{u}}_3 \times \hat{\mathbf{u}}_2))]| =$$

$$\frac{b_2 b_3}{|(\mathbf{r}_3 - \mathbf{r}_1)|} |[(\hat{\mathbf{u}}_3 \cdot \hat{\mathbf{u}}_2)^2 - 1]| =$$

$$\frac{b_2 b_3 |\cos^2(\theta_2) - 1|}{b_2^2 + b_3^2 - 2b_2 b_3 \cos(\theta_2)} = \frac{b_2 b_3 \sin^2(\theta_2)}{b_2^2 + b_3^2 - 2b_2 b_3 \cos(\theta_2)} \tag{A.8}$$

Appendix B. Jacobian for the Dimer Flip Move

The evaluation of the Jacobian of eq 14 becomes easier if the transformation is performed in two steps:

$$\{\mathbf{r}_2,\mathbf{r}_3\} \xrightarrow{\mathrm{A}} \{\mathbf{r}_2,l_{13},b_4,\omega_3\} \xrightarrow{\mathrm{B}} \{b_2,b_3,\omega_2,l_{13},b_4,\omega_3\} \tag{B.1}$$

We have (see Figure 5)

$$\frac{\partial \mathbf{r}_3}{\partial l_{13}} = \frac{\partial(\mathbf{r}_3 - \mathbf{r}_1)}{\partial l_{13}} = \frac{\mathbf{r}_3 - \mathbf{r}_1}{l_{13}} = \frac{\mathbf{b}_2 + \mathbf{b}_3}{l_{13}} = \frac{b_2\hat{\mathbf{u}}_2 + b_3\hat{\mathbf{u}}_3}{l_{13}} \tag{B.2}$$

$$\frac{\partial \mathbf{r}_3}{\partial \omega_3} = \frac{\mathbf{b}_4 \times (\mathbf{b}_2 + \mathbf{b}_3)}{|(\mathbf{r}_4 - \mathbf{r}_1)|} = \frac{\mathbf{b}_4 \times \mathbf{b}_2 + \mathbf{b}_4 \times \mathbf{b}_3}{|(\mathbf{r}_4 - \mathbf{r}_1)|} = \frac{b_4 b_2(\hat{\mathbf{u}}_4 \times \hat{\mathbf{u}}_2) + b_4 b_3(\hat{\mathbf{u}}_4 \times \hat{\mathbf{u}}_3)}{|(\mathbf{r}_4 - \mathbf{r}_1)|} \tag{B.3}$$

$$\frac{\partial \mathbf{r}_3}{\partial b_4} = -\hat{\mathbf{u}}_4 \tag{B.4}$$

where $\hat{\mathbf{u}}_2$, $\hat{\mathbf{u}}_3$, and $\hat{\mathbf{u}}_4$ are unit vectors along the bonds $\mathbf{b}_2$, $\mathbf{b}_3$, and $\mathbf{b}_4$, respectively. Combination of eqs B.2 and B.3 results in the following expression:

$$J_A = \left|\left(\frac{\partial \mathbf{r}_3}{\partial l_{13}}\right)^T \left(\frac{\partial \mathbf{r}_3}{\partial \omega_3}\right)^T \left(\frac{\partial \mathbf{r}_3}{\partial b_4}\right)^T\right| = \left|\begin{vmatrix} \dfrac{(\mathbf{b}_2 + \mathbf{b}_3)}{l_{13}} \\ \dfrac{\mathbf{b}_4 \times (\mathbf{b}_2 + \mathbf{b}_3)}{|(\mathbf{r}_4 - \mathbf{r}_1)|} \\ -\hat{\mathbf{u}}_4 \end{vmatrix}\right| = \frac{1}{|(\mathbf{r}_4 - \mathbf{r}_1)||(\mathbf{r}_3 - \mathbf{r}_1)|} |(\mathbf{b}_2 + \mathbf{b}_3)\cdot([\mathbf{b}_4 \times (\mathbf{b}_2 + \mathbf{b}_3)] \times \hat{\mathbf{u}}_4)| \quad \text{(B.5)}$$

The Jacobian for the second transformation is the same as for the simple flip move (Appendix A):

$$J_B = \frac{b_2 b_3}{|(\mathbf{r}_3 - \mathbf{r}_1)|} |[\hat{\mathbf{u}}_2\cdot(\hat{\mathbf{u}}_3 \times (\hat{\mathbf{u}}_3 \times \hat{\mathbf{u}}_2))]| \quad \text{(B.6)}$$

Substitution of eqs B.5 and B.6 in eq B.1 results in

$$J_{DF} = J_B J_A = \frac{b_2 b_3}{|(\mathbf{r}_4 - \mathbf{r}_1)||(\mathbf{r}_3 - \mathbf{r}_1)|^2} |(\mathbf{b}_2 + \mathbf{b}_3)\cdot ([\mathbf{b}_4 \times (\mathbf{b}_2 + \mathbf{b}_3)] \times \hat{\mathbf{u}}_4)| \, |\hat{\mathbf{u}}_2\cdot[\hat{\mathbf{u}}_3 \times (\hat{\mathbf{u}}_3 \times \hat{\mathbf{u}}_2)]| = \frac{b_2 b_3 b_4}{l_{14}} \sin^2(\theta_2)\left(1 - \left(\frac{\mathbf{l}_{13}\cdot\hat{\mathbf{u}}_4}{l_{13}}\right)^2\right) \quad \text{(B.7)}$$

Extending the above reasoning, it is easy to derive the Jacobian for the n-mer flip move as the product of $n - 1$ Jacobians of type J_A concerning mers 3,...n, $n + 1$, and a last Jacobian of type J_B concerning mer 2:

$$J_{nF} = J_{B,2} \prod_{j=3}^{n+1} J_{A,j}$$

$$= \frac{b_2 b_3}{|(\mathbf{r}_3 - \mathbf{r}_1)|} |\hat{\mathbf{u}}_2\cdot[\hat{\mathbf{u}}_3 \times (\hat{\mathbf{u}}_3 \times \hat{\mathbf{u}}_2)]| \prod_{j=3}^{n+1} \frac{1}{|(\mathbf{r}_{j+1} - \mathbf{r}_1)||(\mathbf{r}_j - \mathbf{r}_1)|} |(\sum_{i=2}^{j} \mathbf{b}_i)\cdot([\mathbf{b}_{j+1} \times (\sum_{i=2}^{j} \mathbf{b}_i)] \times \hat{\mathbf{u}}_{j+1})|$$

$$= \frac{\sin^2(\theta_2)^{n+2}}{l_{1(n+2)}} \prod_{j=2}^{n+2} b_j \prod_{j=3}^{n+1} \left[1 - \left(\frac{\mathbf{l}_{1j}\cdot\hat{\mathbf{u}}_{j+1}}{l_{1j}}\right)^2\right] \quad \text{(B.8)}$$

References and Notes

(1) Bates, F. S.; Wignall, G. D.; Koehler, W. C. *Phys. Rev. Lett.* **1985**, *55*, 2425.
(2) Banaszak, M.; Petsche, I. B.; Radosz, M. *Macromolecules* **1993**, *26*, 391.
(3) Reichart, G. C.; Graessley, W. W.; Register, R. A.; Krishnamoorti, R.; Lohse, D. J. *Macromolecules* **1997**, *30*, 3363.
(4) White, J. L.; Brant, P. *Macromolecules* **1998**, *31*, 5424.
(5) White, J. L.; Lohse, D. J. *Macromolecules* **1999,** *32,* 958.
(6) Jeon, H. S.; Lee, J. H.; Balsara, N. P.; Newstein, M. C. *Macromolecules* **1998**, *31,* 5340.
(7) Vacatello, M.; Avitabile, G.; Corradini, P.; Tuzi, A. *J. Chem. Phys.* **1980***, 73,* 548.
(8) Frenkel, D.; Mooij, G. C. A. M.; Smit, B. *J. Phys.: Condens. Matter* **1992**, *4*, 3053.
(9) Siepmann, J. I.; Frenkel, D. *Mol. Phys.* **1992**, *75,* 59.
(10) de Pablo, J. J.; Laso, M.; Siepmann, J. I.; Suter, U. W. *Mol. Phys.* **1993**, *80,* 55.
(11) Mavrantzas G. V.; Theodorou, D. N. *Macromolecules* **1998**, *31*, 6310.
(12) Dodd, L. R.; Boone, T. D.; Theodorou, D. N. *Mol. Phys.* **1993**, *78,* 961.
(13) Pant, P. V. K.; Theodorou, D. N. *Macromolecules* **1995**, *28*, 7224.
(14) Karayiannis, N. Ch.; Mavrantzas, V. G.; Theodorou, D. N. *Phys. Rev. Lett.* **2002**, *88,* 105503.
(15) Theodorou, D. N. In Nielaba, P.; Mareschal, M.; Ciccotti, G. *Bridging Time Scales: Molecular Simulations for the Next Decade;* Springer-Verlag: Berlin, 2002; p 67.
(16) Karayiannis, N. Ch.; Giannousaki, A. E.; Mavrantzas, V. G. *J. Chem. Phys.* **2003**, *118,* 2451.
(17) Macedonia, M. D.; Maginn, E. J. *Mol. Phys.* **1999**, *96,* 1375.
(18) Martin, M. G.; Siepmann, J. I. *J. Phys. Chem. B* **1999**, *103,* 4508.
(19) Gō, N.; Scheraga, H. A. *Macromolecules* **1970**, *3*, 178.
(20) Mavrantzas, V. G.; Boone, T. D.; Zervopoulou, E.; Theodorou, D. N. *Macromolecules* **1999**, *32*, 5072.
(21) Wu, M. G.; Deem, M. W. *J. Chem. Phys.* **1999**, *111*, 6625.
(22) Allen, M. P.; Tildesley, D. J. *Computer Simulation of Liquids;* Clarendon Press: Oxford, 1987.
(23) Karayiannis, N. Ch.; Giannousaki, A. E.; Mavrantzas, V. G.; Theodorou, D. N. *J. Chem. Phys.* **2002**, *117,* 5465.
(24) Martin, M. G.; Siepmann, J. I. *J. Phys. Chem. B* **1998**, *102,* 2569.
(25) Mattice, W. L.; Suter, U. W. *Conformational Theory of Large Molecules*; John Wiley & Sons: New York, 1994.
(26) Han, J. S.; Lohse, J. D.; Condo, P. D.; Sperline, H. L. *J. Polym. Sci., Part B* **1999**, *37,* 2835.

MA048364P